PERGAMON

Journal of Atmospheric and Solar-Terrestrial Physics 63 (2001) 1559–1569

Journal of ATMOSPHERIC AND SOLAR-TERRESTRIAL PHYSICS

www.elsevier.com/locate/jastp

Zonal neutral winds at equatorial and low latitudes

C. Martinis[a,b], J. Meriwether[c], R. Niciejewski[d], M. Biondi[e], C. Fesen[f], M. Mendillo[a,*]

[a] *Center for Space Physics, Boston University, 725 Commonwealth Ave, Boston, MA 02215, USA*
[b] *Departamento de Física, F.C.E.yT., Universidad Nacional de Tucumán and CONICET, Argentina*
[c] *Department of Physics and Astronomy, Clemson University, Clemson, SC, USA*
[d] *Space Physics Research Lab, University of Michigan, Ann Arbor, MI, USA*
[e] *Department of Physics & Astronomy, University of Pittsburgh, Pittsburgh, PA, USA*
[f] *Center for Space Sciences, University of Texas at Dallas, TX, USA*

Received 1 November 2000; received in revised form 20 February 2001; accepted 5 March 2001

Abstract

Fabry–Perot interferometric (FPI) measurements of thermospheric zonal neutral winds at Arequipa, Peru (16.7°S, 71.5°W, −2.7° dip), and Carmen Alto, Chile (23.1°S, 69.4°W, −10.2° dip), were collected during the solar minimum periods of September–October 1996 and 1997. The data set included 39 nights from Arequipa and 14 nights for Carmen Alto, with 8 nights of simultaneous observations. Analysis of averaged results found the peak evening zonal neutral wind speed of $\sim 127 \pm 15$ m/s eastward for the Arequipa observatory, which is located near the magnetic equator, to occur between 21:30 and 22:30 LT. In contrast, the peak evening zonal winds of $\sim 100 \pm 10$ m/s eastward observed from Carmen Alto, which is located near the crest of the equatorial ionization anomaly (EIA), occurred ~0.5–1 h later. These measurements represent the first case of groundbased FPI observations of the so called equatorial temperature and wind anomaly (ETWA) over such a small latitude range in the same longitude sector. This reduction in speed of ~20–25% at Carmen Alto relative to Arequipa is attributed to increased ion drag at Carmen Alto caused by the higher electron density within the EIA region at altitudes of 220–300 km. Model studies were conducted using electron density and neutral atmosphere parameters form the parameterized ionospheric model (PIM) and the mass spectrometer incoherent scatter (MSIS) models, respectively, to calculate the ratio of ion–neutral collision frequencies at the two sites. We found that the increase in electron density within the EIA was sufficient to account for the observed reduction in the zonal wind. Thus, this analysis confirms the dominant role of ion drag in modulating thermospheric dynamics at equatorial latitudes. A comparison of the FPI results with the predictions by two current neutral wind models, the Horizontal Wind Model-90 and the NCAR Thermospheric Ionosphere Electrodynamics General Circulation Model (TIEGCM), reveals that neither is able to reproduce accurately the latitude dependence reported here. Model refinements for electrodynamics and improved resolution are suggested.

Keywords: Equatorial ionization anomaly; Equatorial aeronomy; Thermospheric winds; Ion drag

1. Introduction

The equatorial ionization anomaly (EIA) is characterized by a local minimum in ionospheric densities at the magnetic equator with two crests on either side at 12–20° dip latitude (N or S), depending on solar flux levels. Martyn (1953) suggested that the cause of this anomaly was an upward $\mathbf{E} \times \mathbf{B}$ drift of the equatorial ionospheric plasma, followed by diffusion along magnetic field lines to lower altitudes at higher latitudes. Subsequent modeling (e.g., Anderson, 1973) verified the electrodynamical origin of the F-region equatorial trough and tropical crests that dominate low latitude ionospheric morphology.

* Corresponding author. Tel.: +1-617-353-2629; fax: +1-617-353-6463.
E-mail address: mendillo@bu.edu (M. Mendillo).

1364-6826/01/$ - see front matter
PII: S1364-6826(01)00022-0

Hedin and Mayr (1973) suggested a corresponding equatorial neutral wind and temperature anomaly in the same region. The effect of the enhanced ion densities within each crest is increased ion-drag which reduces the neutral wind speed and increases neutral temperatures at the crests. Raghavarao et al. (1991) provided the first observations of this effect in this analysis of neutral wind and temperature data from the Dynamics Explorer-2 satellite. The in situ observations were made by the wind and temperature spectrometer (WATS) instrument sampling in the 300–450 km altitude range. The zonal winds exhibited a broad maximum centered on the dip equator, with minima on either side at 15–20° dip latitude. These two minima were nearly collocated with the crests of the EIA, and the maximum was located at the trough of the EIA. Their results showed neutral winds speeds reduced by as much as 50–60 m/s at the crests at 12:00 and 19:00 LT. In a subsequent study, Raghavarao et al. (1998) describe the average local time variations in the zonal winds versus latitude during the low solar flux period of 1981–1982. They calculated differences in the wind velocities at the crests (located at 16–18° dip latitude) and trough of the ionization anomaly for both day and night periods. The magnitude of the differences was found to be proportional to the EIA peak electron density, with the zonal wind values at the crest usually half the equatorial values. They compared these differences with the NASA Horizontal Wind Model (HWM-90) and found that it did not portray the observed morphology under the solar maximum conditions studied.

To date, the behavior of low latitude zonal winds has been studied by comparing ground-based FPI measurements at only a few sites, i.e., Arequipa, Peru (16°S, −3° dip latitude), Arecibo, Puerto Rico (17°N, 29° dip latitude), and Sao Jose dos Campos (23°S, −16° dip latitude), Brazil. Fig. 1 shows the locations of these sites. Biondi et al. (1990) compared Arequipa Fabry–Perot neutral wind measurements near the magnetic equator in the Peruvian sector with simultaneous measurements at Sao Jose dos Campos within the EIA of the Brazilian sector. They found the winds for the three nights examined to be similar in magnitude, thus suggesting a negligible latitude dependence as sampled at longitudes on opposite sides of the continent. Winds at nearly the same geographic latitudes in opposite hemispheres were compared by Biondi et al. (1999), using the FPI observatories of Arequipa and Arecibo. They also compared their measurements with results from the TIEGCM model. Qualitative areas of agreement were found, but there were also periods of considerable differences that were attributed to the very different ion drag at the two sites. Thus in both Biondi et al. (1990, 1999) studies, it was noted that the large differences in the evening and nighttime plasma density profiles at Arequipa and the other two locations (−3° dip versus +29° and −16° dip, respectively) would produce differing ion drag effects.

Wu et al. (1994) investigated the local time and longitudinal variations of thermospheric neutral winds using DE data,

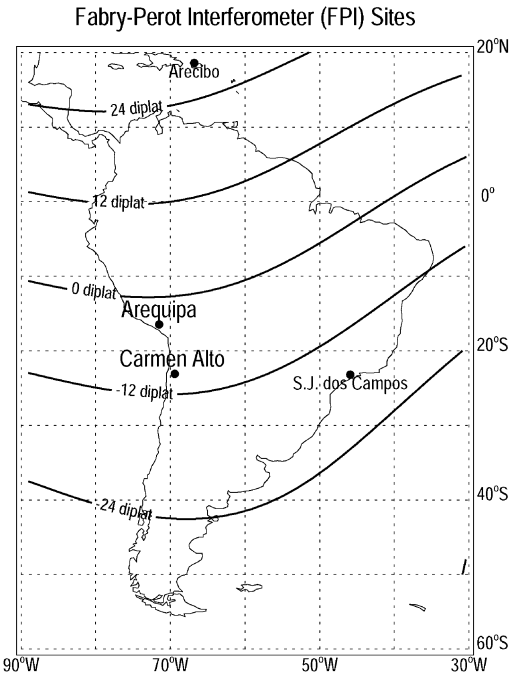

Fig. 1. Locations of the FPI sites at Arequipa and Carmen Alto with respect to geographic and geomagnetic coordinate systems. Also shown are Arecibo and S.J. dos Campos, sites used in previous FPI studies. The Equatorial Ionization Anomaly (EIA, often called the Appleton Anomaly) refers to low F-region electron densities near the geomagnetic equator (0° dip latitude) in comparison to crests found in the 12–24° dip latitude range in both hemispheres.

averaged in bands of ±9° in geographic latitudes. While their analysis method suppressed latitude effects, the work is an interesting review of thermospheric winds and the role of ion drag. For example, in the South Atlantic magnetic anomaly (SAA) region (∼20–40°W) the zonal winds were slowest, probably due to the larger plasma densities of the SAA and the southern EIA crest falling within their latitude bin (see Fig. 1).

In this study, we report the first ground-based FPI neutral wind measurements from two low latitude sites in the same hemisphere and in the same longitude sector. These measurements sample simultaneously the thermospheric winds at two locations (dip latitudes −10.2° and −2.7°) during times when peak F-region densities at the two sites differs by nearly an order of magnitude. Therefore, reduced neutral winds would be expected to occur at the site closer to the crest of the EIA.

2. Observations

Fabry–Perot interferometers (FPI) in Arequipa, Peru (17°S, 71°W, −2.7° dip latitude), and Carmen Alto, Chile (23°S, 69°W, −10.2° dip latitude), provided neutral wind

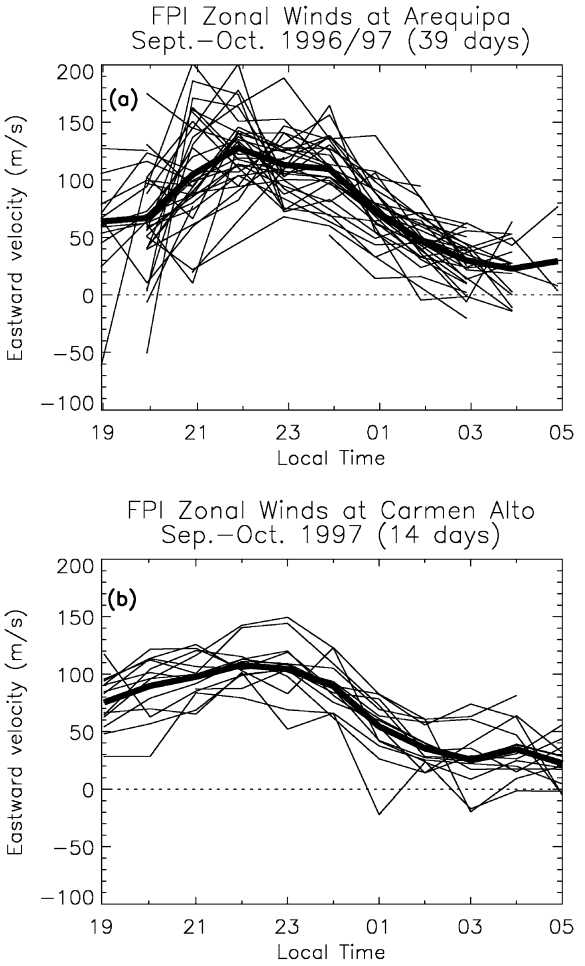

Fig. 2. FPI neutral wind measurements during September–October, 1996–1997. (a) Arequipa (b) Carmen Alto. The thin lines indicate individual days and the thick lines indicate the average.

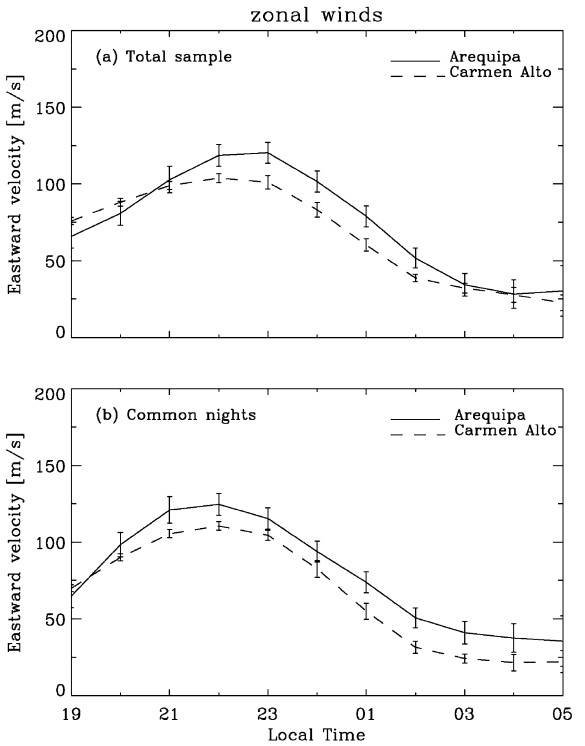

Fig. 3. (a) Averaged neutral winds at both sites. (b) Same as (a) but for 8 common nights. The common night data are representative of the larger data set and will be used in subsequent model comparisons.

data for this study (see Fig. 1). Measurements from the Arequipa FPI were from September to October 1996 and 1997, while measurements from Carmen Alto were available only for September–October 1997. Only nights with low to moderate geomagnetic activity ($K_p < 4$) were analyzed.

The Arequipa FPI acquired data at approximately 20–30 min intervals with a measurement error of $\sim$15 m/s for each line-of-sight Doppler determination. The observing sequence was a cycle of observations at 30° elevation that included the zenith and four azimuthal directions that were shifted in azimuth by 14° counter-clockwise relative to the cardinal positions. This was done to facilitate bistatic simultaneous measurements with Carmen Alto, the subject of a separate investigation. The zenith measurements are used to generate a zero wind Doppler reference for use in the Doppler shift determinations utilizing the fact that horizontal thermospheric wind component speeds are generally one to two orders of magnitude larger than the vertical component, whose nightglow average is taken to be close to zero velocity. Meriwether et al. (1997) provides more details on the measurement technique and wind calculations.

The Carmen Alto FPI had a detector of greater sensitivity than the Arequipa FPI instrument. It acquired data at approximately 10 min intervals with a measurement error of $\sim$ 10 m/s for each point. Reliable measurements were obtained at 30° elevation for the four cardinal directions, and in the direction toward Arequipa at $\sim$351° azimuth. The analysis approach adopted was to assume the neutral zonal wind field was uniform over the instrument field of view. The Carmen Alto FPI results were analyzed to produce average zonal wind speeds.

Fig. 2 shows the winds obtained at each site for the periods of study (see Table 1). Panel (a) comprises 39 nights of data at Arequipa and panel (b) 14 days at Carmen Alto. The averaged patterns are shown in Fig. 3(a). Since the Carmen Alto site operated for only a 7 week period in 1997, there were only eight nights in September (days 239–246) with data available from both sites. We conducted several tests to see if the common-night data were, in fact, representative of the total sample, as might be expected for solar minimum conditions at a single site. The results for the 8 night

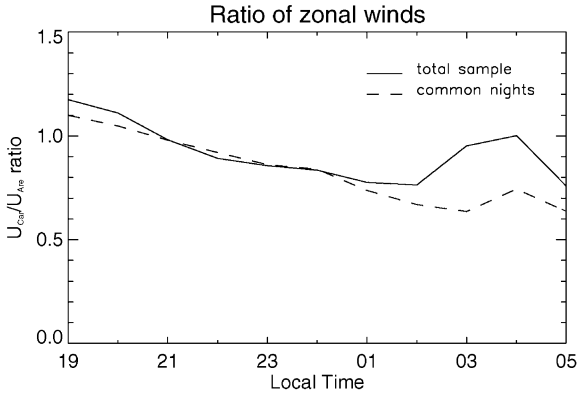

Fig. 4. Ratios of zonal winds observed at Carmen Alto and Arequipa for the full and common data sets shown in Fig. 3. The common night values, which show a smoother behavior than the larger statistical sample, will be the basis for comparison with the models.

Table 1
Summary of FPI data used from Arequipa and Carmen Alto

	All data		Common data	
Site	Are	Car	Are	Car
# of days	39 (1996–1997)	14 (1997)	8 (1997)	8 (1997)
$\langle K_p \rangle$	1.9	1.2	2.4	2.4
$\langle$F10.7$\rangle$	82	90	95	95
Variability (m/s)	35	22	35	22

average patterns are shown in Fig. 3(b). These averaged curves behave almost identically to the ones showed in Fig. 3(a), between 21:00 LT and $\sim$ 02:00 LT, as did the night-by-night comparisons. Error bars in Fig. 3 are computed considering the error in the individual measurements and the error in the calculation of the average values for each local time. Fig. 4 shows the ratio of neutral zonal winds at the two sites for both data sets.

We conclude from Figs. 3 and 4 that the averaged zonal winds at Arequipa are larger than the Carmen Alto winds by $\sim$ 20–25%. Both stations show maxima between 21:30 and 23:00 LT, with peak values of $\sim$ 127 and $\sim$ 100 m/s for Arequipa and Carmen Alto, respectively. In addition, the Arequipa zonal winds show greater variability, as shown visually in Fig. 2 and quantitatively in Table 1.

3. Ion drag effects in the 630 nm airglow region

Using plasma drift observations from the DE-2 satellite combined with F-region dynamo theory, Anderson et al. (1987) found the latitude dependence of the zonal thermospheric wind component to be represented by the empirical formula

$$U = U_{EQ} \cos(4\phi) \tag{1}$$

at 23:00 LT during solar maximum conditions, where ϕ is the dip latitude and U_{EQ} is the neutral zonal wind at the magnetic equator. This representation of winds in the EIA region had been suggested by Anderson and Mendillo (1983) to explain the westward tilt of depleted flux tubes detected via ground-based airglow imaging (Mendillo and Tyler, 1983).

Eq. 1 at 23:00 LT predicts a neutral wind ratio of $U_{car}/U_{are} = 0.77$ (applicable to solar maximum conditions). Our FPI observations—during solar minimum conditions—show a value of $U_{car}/U_{are} \sim 0.85$ at that time. Thus, the FPI observations show a reduction in zonal neutral wind comparable to the empirical prediction, even for rather different solar conditions.

To examine the possibility that the differences in the neutral winds at the two locations can be attributed to increased ion-drag near the crests of the anomaly (Hedin, 1973; Raghavarao et al., 1991, 1998), we have calculated the ion drag term in the momentum balance equation for both locations. Ion-drag is defined as the force per unit volume on the neutrals due to the collisional interactions of the neutral gas with the plasma. It can be described mathematically as

$$\mathbf{F} = \rho \nu_{ni} (\mathbf{U} - \mathbf{V}) \tag{2}$$

where ρ is the mass density, ν_{ni} is the collision frequency for momentum transfer from the neutral gas to the ions, $\mathbf{U}$ is the neutral velocity and $\mathbf{V}$ is the plasma velocity. Assuming that the only external force to balance the thermospheric pressure gradient force (grad)P is ion-drag, the steady-state momentum balance equations at the latitudes of the two FPI observations are given as a first approximation by

$$\begin{aligned} \text{grad } P_{are} &= [\rho \nu_{ni} \mathbf{U}(1 - \Pi)]_{are}, \\ \text{grad } P_{car} &= [\rho \nu_{ni} \mathbf{U}(1 - \Pi)]_{car}, \end{aligned} \tag{3}$$

where Π is a polarization coefficient, defined as $\mathbf{V}/\mathbf{U}$ (Rishbeth, 1971). For our calculations we will assume that this coefficient is similar for both sites. If the neutral pressure gradient force and the mass density are assumed to be the same at both sites, the ratio of the neutral winds at the two latitudes of Carmen Alto and Arequipa becomes

$$\frac{U_{car}}{U_{are}} = \frac{\nu_{ni}^{are}}{\nu_{ni}^{car}}. \tag{4}$$

The collision frequency is represented by Rishbeth (1972) as

$$\nu_{ni} = K_{ni} N_i, \tag{5}$$

where N_i is the ion concentration, and the coefficient K_{ni} is the rate of momentum transfer per unit volume and depends on the species involved. For the dominant O^+ ions, K_{ni} is

given (Schunk and Nagy, 2000) as

$$K_{ni} = 3.67 \times 10^{-17} \times T_r^{0.5}[1 - 0.064 \times \log T_r]^2 \ (m^3/s), \tag{6}$$

where $T_r = (T_n + T_i)/2$ is the average temperature of the neutral particles and ions (in the nighttime ionosphere we can assume that $T_n = T_i$). Substituting these values into Eq. (4), the ratio of the neutral winds between Carmen Alto and Arequipa becomes

$$\frac{U_{car}}{U_{are}} = \frac{N_{i_{are}}}{N_{i_{car}}} \left(\frac{T_{are}}{T_{car}}\right)^{1/2} \left(\frac{1 - 0.064 \log T_{are}}{1 - 0.064 \log T_{car}}\right)^2. \tag{7}$$

To evaluate Eq. (7), electron density ($N_e = N_i$) and neutral temperature values are needed as a function of latitude for the ionosphere–thermosphere height region that produces the 630 nm airglow measured by the FPI's (~250–300 km). Eq. (7) points out that ion drag depends far more strongly on plasma density values than neutral temperatures (with the first temperature term dominant over the second for the range of T_n found in the low latitude thermosphere). For temperatures we used the MSIS-86 predictions of ~800 K at both locations, i.e., no latitudinal variation. The FPI measurements yielded temperatures of 900 K at Arequipa; temperature determination at Carmen Alto was hampered by a loss in the fidelity in the instrument line profile with time, an essential requirement for instrumental characterization necessary for temperature determination. Previous reports of FPI temperatures found values ~100–300 K higher than MSIS predictions at low latitude sites (Biondi and Meriwether, 1985), and thus in using MSIS values there is a small uncertainty introduced; this will be discussed further later.

We have used the parameterized ionospheric model (PIM) (Daniell et al., 1995) to calculate electron density values with $K_p = 2$ and F10.7 = 90 for equinox conditions (day 264). To assess the role of the electron density altitude distributions in Eq. (7), Fig. 5(a) gives the modeled N_e at 250 km and Fig. 5(b) at 300 km for several local times. The arrows mark the dip latitude locations of Arequipa and Carmen Alto. We see that Arequipa lies within a few degrees of the dip equator and Carmen Alto lies, for this model, on the equatorward edge of the southern crest of the ionization anomaly. Fig. 5(a) and (b) predict that the EIA has pronounced altitude dependence, and thus the ion-drag effect upon thermospheric winds in the 630 nm airglow layer can be complex. For example, at 19:30 LT the Arequipa and Carmen Alto N_e values are small, and their ratio is $\sim \frac{1}{10}$ at both heights. At 250 km the anomaly disappears later in the evening, but persists throughout the night at 300 km.

In addition to the latitude patterns shown in Fig. 5(a) and (b), it is important to realize that FPI data come from 630 nm airglow emission, the altitude of which

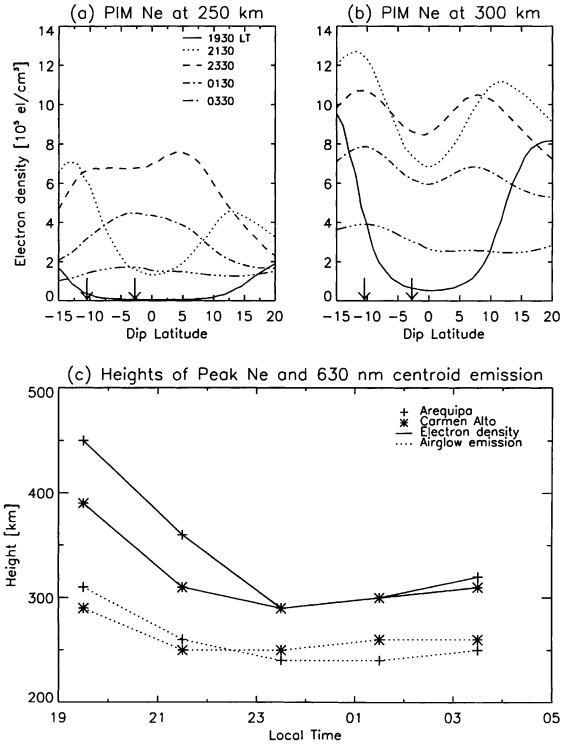

Fig. 5. PIM electron density profiles: (a) at 250 km and (b) at 300 km, illustrating the different behavior of the Appleton Anomaly at bottom-side F layer heights for solar minimum conditions. Arrows indicate locations of the sites. (c) Comparison of the centroids of 630 nm emission (dotted curve) and peak electron density altitudes from PIM (solid curve), using $N_e(h)$ profiles at Arequipa (+) and Carmen Alto (∗).

is not constant throughout the night. We determined the peak airglow emission and centroid airglow heights using standard F-region airglow theory (e.g., see Semeter et al., 1996; Meriwether et al., 1997). The resulting volume emission rates versus altitude profiles are roughly Gaussian, and thus one can approximate the centroid airglow height by the median height of the airglow layer. The peak electron density altitudes (hm_{N_e}) and the centroid altitudes (h_{cen}) are given in Table 2 for different local times throughout the night. The centroid altitudes obtained agree with previous calculations for similar solar conditions (Meriwether et al., 1997). Fig. 5(c) displays both the centroid airglow heights and the peak F-region altitudes. It is interesting to note that early in the evening, hm_{N_e} is significantly larger than h_{cen}. This result was also found by Meriwether et al. (1997) in their calculations of 630 nm volume emission profiles for Arequipa. This difference is greater for the latitude of Arequipa, resulting in an even larger difference in the electron density between Carmen Alto and

Table 2
Heights of the $N_e(h)$ peak density and the 630 nm centroid emission, with corresponding N_e values and integrated airglow brightness at Arequipa and Carmen Alto

Time	Height (km)				Electron density ($\times 10^5$ cm^{-3})				Column integrated	
	hm_{N_e}		h_{cen}		At hm_{N_e}		At h_{cen}		emission ε_{630} (Rayleighs)	
LT	ARE	CAR	ARE	CAR	ARE	CAR	ARE	CAR	ARE	CAR
19:30	450	390	310	290	10.0	14.0	0.8	3.2	9.8	47.3
21:30	360	310	260	250	9.8	12.7	2.5	6.3	96.5	206.6
23:30	290	290	240	250	8.7	10.7	5.5	6.6	180.4	154.4
01:30	300	300	240	260	6.2	7.9	3.47	4.6	114.3	82.4
03:30	320	310	250	260	6.0	3.9	1.7	2.11	49.3	40.5

Arequipa than that caused by the ionization anomaly at fixed heights.

From Eq. (4), the ratio of collision frequencies represents the ratio of the neutral wind values. From Eq. (7), this ratio is equal to the electron densities' ratio, if the temperatures at both sites are equal. With this assumption, we calculated the neutral winds' ratio at the centroid height of 630 nm and along a path through the altitude-dependent emission layer. For the latter case, a weighted collision frequency is calculated by

$$\langle \nu_{ni} \rangle = \frac{\sum_j \varepsilon_j \nu_j}{\sum_j \varepsilon_j}, \tag{8}$$

where ε_j is the volume emission rate at the level j. Calculations are made every 10 km, from 200 to 320 km, except early in the night (19:30 LT), where calculations were made from 220 to 380 km.

4. Comparison with observations

Table 3 lists values of the ratio of calculated winds (U_{car}/U_{are}) using Eq. (7), with equal neutral temperature values, for a local time range from post-sunset to pre-dawn. In the last column of Table 3 we compare the model results with the observed wind patterns for the common nights shown in Fig. 4.

The observed wind ratios decrease smoothly from $\sim$1 early in the night to $\sim$0.6 prior to dawn. From Table 2 we can see that at 19:30 LT the N_e values at the centroid altitudes are small at both sites. Ion drag effects are consequently very small, and hence the relative difference in N_e does not impose any latitudinal dependence upon the winds. Consequently the winds are large at both sites and their ratio is close to 1. Later on, when the EIA is fully developed and the electron densities in the airglow layer reach their maximum values (21:30–23:30 LT), the winds respond to ion-drag and their ratio decreases. Thus, by midnight, the observed and calculated ratios are comparable at $\sim$0.9. As described in the next section, the ion drag mechanism involves a time delay of the order of 1–2 h; the winds will not respond to the influence of the ions instantaneously, and that influence will be enhanced by the larger ion concentrations later in the night.

5. Comparison with models

There are two types of thermospheric wind models that are widely used by the aeronomy community: (1) the empirical Horizontal Wind Models (HWM-87 and HWM-90) (see Hedin et al., 1991), and (2) theoretical, self-consistent, general calculation models, such as the TIEGCM (see Richmond et al., 1992). We have examined both models to see if they portray the types of wind speeds versus time and latitude found in our measurements. Model outputs from TIEGCM came from runs simulating equinoctial conditions for low solar and geomagnetic

Table 3
Calculated and observed wind ratios using different 630 nm emission heights

Time	Calculated U_{car}/U_{are}		Observed U_{car}/U_{are}
LT	At 630 nm centroid emission	At 630 nm height weighted emission	Common nights
19:30	0.25	0.3	1.05 ± 0.23
21:30	0.40	0.5	0.89 ± 0.16
23:30	0.83	0.85	0.90 ± 0.17
01:30	0.75	0.89	0.71 ± 0.23
03:30	0.80	0.84	0.62 ± 0.36

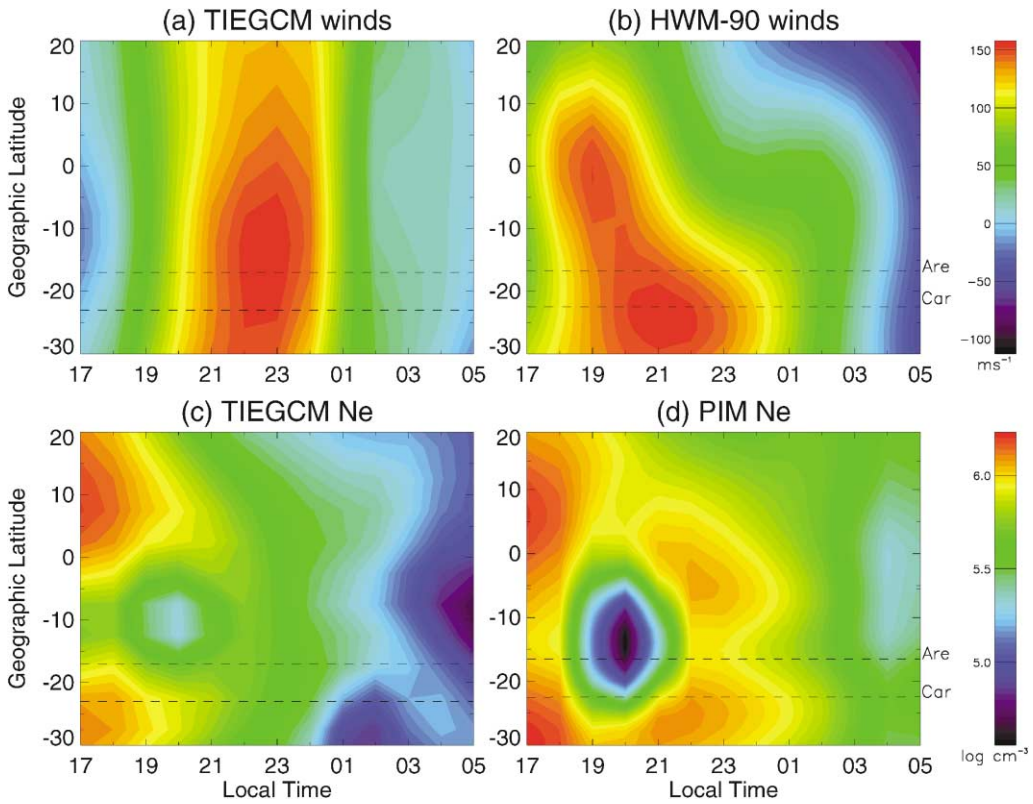

Fig. 6. Thermospheric model outputs for equinox, low magnetic activity and solar minimum conditions: (a) TIEGCM winds, (b) HWM-90 winds, (c) TIEGCM N_e, and (d) PIM N_e.

activity (Fesen et al., 2000). The Fesen et al. (2000) results represent state-of-the-art simulations for equatorial aeronomy. In particular, these runs were tuned to reproduce the post-sunset electrodynamical drift patterns at Jicamarca, Peru. Thus, they are well suited for additional comparisons with the thermospheric neutral winds patterns described here for the same longitude sector.

TIEGCM results for zonal winds at 300 km along the geographic meridian (75°W) closest to the Arequipa–Carmen Alto sites are given in Fig. 6(a); Fig. 6(b) portrays the zonal neutral winds produced by the HWM-90 model for the same equinoctial conditions with low solar and geomagnetic activities. The corresponding electron densities at 300 km from TIEGCM and PIM are shown in Figs. 6(c) and (d). Recall that the equatorial and low latitude results from PIM (Daniell et al., 1995) come from the parameterization of output from the theoretical model of Anderson (1973), a model that uses MSIS for thermospheric densities and temperatures and HWM-90 for neutral winds. It is not a self-consistent model and thus, while winds can re-distribute plasma, there is no feedback of plasma ion drag upon the winds.

There is a rich set of comparisons to be made from the model output shown in Fig. 6. Consider first the neutral winds in panels (a) and (b). Fig. 6(a) shows that a negligible latitude gradient in TIEGCM winds occurs throughout the equatorial region. Thus, there is no "equatorial wind anomaly" in TIEGCM. Yet, as Fig. 6(c) shows, electrodynamical processes are clearly evident, with a well formed N_e anomaly at 300 km having a trough at the geomagnetic equator (~11°S) and crests at ±20–25° to either side. While the time dependence of the overall ion drag effect upon the winds appears to be correct, i.e., the wind speeds increase as the plasma densities decrease, the model does not portray the observed latitude effect in zonal winds. For HWM-90 (panel b) there is a 10–20 m/s latitude gradient in the winds between the Arequipa and Carmen Alto sites after 20:00 LT, but in the opposite sense to that observed (Fig. 3). Also, early in the night (~ 19:00 LT), the HWM winds are 2–3 times larger than observed.

A comparison of Figs. 6(c) and (d), portraying N_e at 300 km from TIEGCM and PIM, respectively, shows that the EIA pattern disappears after 22:00–23:00 LT in the NCAR model, while it is still present until 03:00 LT in PIM. This suggests that the electrodynamical drift, computed self-consistently in the TIEGCM, might be insufficient to establish a latitudinal structure capable of exerting the

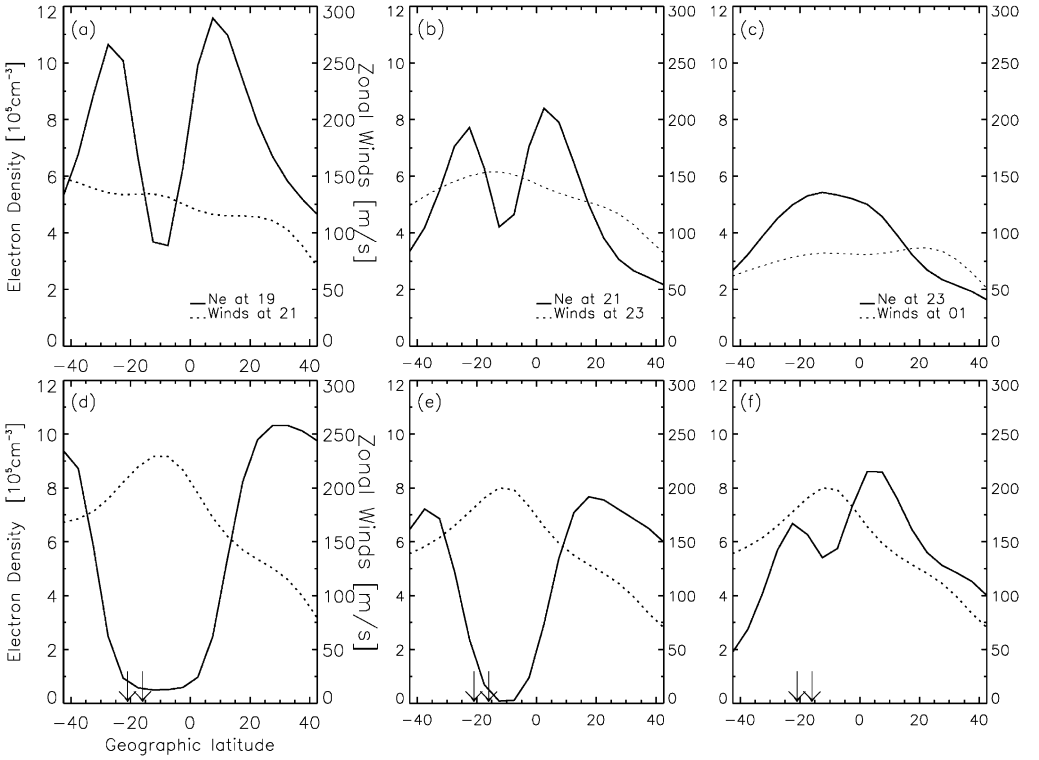

Fig. 7. TIEGCM predicted winds and electron densities at 300 km and different local times. Panels (a), (b), and (c), for F10.7 = 85, predicting little difference in the zonal winds at the latitudes of the two sites. Panels (d), (e), and (f), for F10.7 = 200, predicting a stronger latitudinal variation in the zonal winds. As in Fig. 5 the arrows show the FPI locations.

regional ion drag effects needed to reduce non-equatorial zonal winds. It should be noted that the separation of the sites ($\sim 7^\circ$ in geographic latitude) is of the order of the 5° latitude grid used in the TIEGCM calculations (discussed further below). In the Fesen et al. (2000) simulations, the calculated vertical drifts were ~15–20 m/s for the post-sunset period. In another run in which the pre-reversal enhancement was suppressed, the EIA did not develop but the winds showed essentially the same uniform pattern as in Fig. 6(a).

As a further assessment of ion drag effects in TIEGCM results at low latitudes, we examined the model output for solar maximum conditions. In order to see the full trans-equatorial development of the Appleton Anomaly, model results spanning fifteen gird points are used to cover the geographic latitude range of $\pm 40^\circ$. Fig. 7 shows output for both solar minimum and solar maximum conditions. Panels (a), (b) and (c) show N_e and zonal winds at 300 km for solar minimum conditions (F10.7 = 85) and panels (d), (e) and (f) at the same height for solar maximum conditions (F10.7=200). We noted from Figs. 6(a) and (c) that equatorial winds respond to the minimum in N_e and, via reduced ion drag, reach a maximum approximately 2 h later. Thus the same time delay is used in Fig. 7, with N_e at 19:00, 21:00 and 23:00 LT and winds at 21:00, 23:00, and 01:00 LT.

Fig. 7 shows that the trans-equatorial crest-to-trough ratios of electron density are of the order of ~100 until ~ 22:00 LT under solar maximum conditions, while under solar minimum conditions this ratio is only ~2–3. Thus, a strong latitudinal dependence of zonal winds is predicted only for solar maximum conditions. This dependence corresponds to the EIA ion drag conditions at the 630 nm centroid emission height. It is interesting to note that the differences in winds at the grid points corresponding to Arequipa and Carmen Alto are very small in these solar maximum simulations, probably due to the broad extent of the ionization trough.

Returning to the solar minimum conditions of relevance to our observations, we address the issue of why the PIM electron densities used in our scaling analysis of ion drag (Eq. (7) and Table 3) led to a satisfactory latitude gradient in winds, while the self-consistent model (TIEGCM) did not. To do this we concentrated on the bottom-side profiles where the 630 nm airglow signatures observed by the FPI's are generated. In Fig. 8, the $N_e(h)$ profiles at the same grid points used by TIEGCM (Long 70°W, Lat 17.5°S and 22.5°S for Arequipa and Carmen Alto, respectively) are given at several local times from both models. The left panels show $N_e(h)$ from TIEGCM and the right panels $N_e(h)$

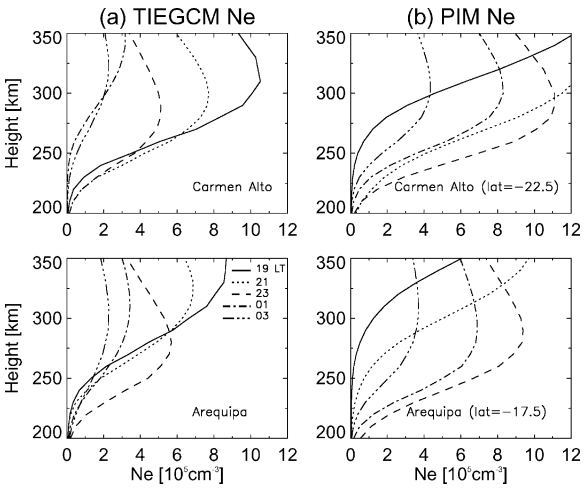

Fig. 8. $N_e(h)$ profiles at solar minimum conditions from (a) TIEGCM and (b) PIM at the same grid points: 75°W, 22.5°S (upper panel), and 75°W, 17.5°S (lower panel), showing differing electron density patterns in the 630 nm airglow nightglow emission layer (see text).

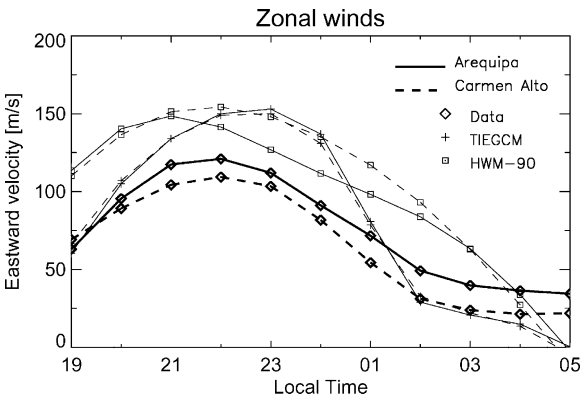

Fig. 9. Summary of zonal wind observations and simulations results. Solid and dashed lines represent Arequipa and Carmen Alto, respectively, obtained from FPI observations, HWM-90 model, and TIEGCM model.

from PIM. The time evolution pattern is clearly different for the two models at both Carmen Alto, upper panel, and Arequipa, lower panel. At 250–300 km ($\sim$ the centroids of 630 nm emission), the Carmen Alto TIEGCM electron densities reach their maxima at 19:00 LT and decrease afterwards. For the same altitude range, PIM N_e's increase from low values at 19:00 LT to maxima at 23:00 LT, and then decrease. For Arequipa, the temporal behavior is similar for both models, e.g., maxima in N_e at 23:00 LT. But differences appear in the values of the electron densities; a broader electron density range is portrayed by PIM, from $\sim 10^4$ to $\sim 10^6$ cm^{-3}, while TIEGCM results are constrained to 2×10^5 to $\sim 6\times10^5$ cm^{-3}. Carmen Alto PIM densities are also larger throughout the night in comparison to TIEGCM results. Thus, for the TIEGCM, there are no appreciable ion drag effects in the 630 nm airglow layer because the electron densities are too low in magnitude and/or have no latitude gradient over the region sampled. Fig. 9 summarizes the comparison between the observed zonal winds (Fig. 3), the theoretical TIEGCM results (Fig. 6(a)) and the HWM-90M empirical model results (Fig. 6(b)).

6. Conclusions

We have compared thermospheric nighttime zonal neutral winds at two latitude sites in the same longitude sector for the first FPI ground-based study of the equatorial neutral wind anomaly, first identified in satellite data by Raghavarao et al. (1991, 1998). The results after $\sim$ 20:00–21:00 LT show consistently larger zonal winds at Arequipa, located near the geomagnetic equator, in comparison to those at a site $\sim7^\circ$ further poleward (Carmen Alto). These findings are consistent with those of Raghavarao et al. (1998) who used in situ DE instrumentation that provided measurements at heights that were generally higher than the 630 nm layer.

To verify that the latitude pattern of winds is caused by ion drag effects that anti-correlate with the behavior of the equatorial ionization anomaly (EIA), we conducted several scaling and computational exercises relevant to FPI height-dependent airglow observations. Using a simplified form of the momentum equation for the neutrals, the ratios of the zonal wind speeds at the two latitudes are given by the ratios of the ion–neutral collision frequencies. These, in turn, depend on plasma densities and neutral temperatures, which we take from the PIM and MSIS models. The altitude variations in the electron density patterns in the Appleton anomaly proved to be the dominant cause of differences in ν_{ni} at the various heights of the 630 nm layer sampled by the FPIs. The wind ratios computed at the centroid heights of 630 nm emission agreed best with the FPI observations at the two sites.

We were unable to address the issue of the thermospheric temperature anomaly (Peak T_n at N_e crests) reported by Raghavarao et al. (1991, 1998) from our measurements at the two sites due to FPI calibration problems at Carmen Alto. Since the MSIS model gave essentially identical T_n values at both sites, there were no T_n effects on our calculated ν_{ni}. Even if we assume that there is a T_n anomaly of 100–150°K (as reported by Raghavarao et al., 1998), the wind ratios change only $\sim$ 5% due to the weak temperature dependence in the ν_{ni} expression (Eq. (7)). Raghavarao et al. (1991) showed that the pattern of zonal winds observed by DE-2 was not present in the HWM-87 and HWM-90 models. Similarly our FPI observational results disagree with the empirical HWM predictions, presumably because the model did not draw upon FPI data from such closely spaced stations at low latitudes.

Biondi et al. (1999) compared Arequipa FPI zonal wind measurements with TIEGCM patterns for that site and found that, while they agree in their temporal variations, the model values run 20–50 m/s higher than the measurements. Here we have extended such comparisons by using two FPI sites and the most recent published TIEGCM simulations (Fesen et al., 2000) for the low latitude ionosphere (see Fig. 9). We find that the behavior of solar minimum nighttime zonal winds in TIEGCM seems to be insensitive to electrodynamics effects upon the thermosphere. A comparison between PIM and TIEGCM shows that the behavior of N_e is different under the same geophysical conditions, i.e., in PIM the EIA persists during the night, while in TIEGCM it disappears after 20:00 LT. This difference has consequences for ion drag upon the winds. This was verified by noting that the zonal winds obtained from simulations in which the pre-reversal enhancement in the vertical drift was suppressed differed only slightly from the case with vertical drift present. Only under solar maximum conditions did the TIEGCM yield a latitudinal dependence in the wind (Fig. 7). We hope to verify this using multi-site FPI observations during the present solar maximum period. Yet, we note from Fig. 7 that there were very small differences in the TIEGCM predicted solar maximum winds at the grid points corresponding to Arequipa and Carmen Alto.

Finally, the reasons for the shortfall in TIEGCM predictions of latitude-dependent zonal neutral winds at solar minimum conditions are not obvious. Deficiencies in representing ion drag effects may result from N_e versus height and latitude patterns not well portrayed by the TIEGCM. More extensive model validations should be conducted using ionosonde or GPS/TEC data throughout the low latitude region. The use of nested-grid methods (see Wang et al., 1999) in future models, and considerably better latitude resolution in FPI observations, would be needed to accurately portray low latitude ionosphere–thermosphere phenomena at times of both solar minimum and maximum conditions.

Acknowledgements

We are indebted to Tricia Clark for her assistance in the FPI's data analysis and to Henry Rishbeth for helpful discussions.

Funding support for this research was provided by the National Science Foundation CEDAR and NSF Aeronomy programs through Grant awards ATM-9714771, ATM-9714770, and ATM-9414403 to M. Mendillo, J. Meriwether, and M. Biondi, respectively, and Grants ATM 9796035 and 9796036 to C. Fesen. The National Center for Atmospheric Research (NCAR) provided computing time. NCAR is supported by NSF.

Space and on-site technical support for the operations of the FPI instrument at the NASA Satellite Laser Ranging Station at Arequipa, Peru, are provided by the National Aeronautic and Space Administration. Support for the FPI observations in Carmen Alto was provided by the Air Force Research Laboratory and on-site technical assistance was provided by Jorge Araya from Departamento de Física, Universidad Católica del Norte, Antofagasta, Chile.

References

Anderson, D.N., 1973. A theoretical study of the ionospheric F-region equatorial anomaly, II. Results in the American and Asian sectors. Planetary and Space Science 21, 421–442.

Anderson, D.N., Heelis, R.A., McClure, J.P., 1987. Calculated nighttime eastward plasma drift velocities at low latitudes and their solar cycle dependence. Annales Geophysicae 5A, 435–442.

Anderson, D.N., Mendillo, M., 1983. Ionospheric conditions affecting the evolution of equatorial plasma depletions. Geophysical Research Letters 10, 541–544.

Biondi, M.A., Meriwether, J.W., 1985. Measured response of the equatorial thermospheric temperature to geomagnetic and solar flux changes. Geophysical Research Letters 12, 267.

Biondi, M.A., Meriwether, J.W., Sahai, Y., Takahashi, H., 1990. Thermospheric neutral winds at low latitudes during the September–October 1986 SUNDIAL campaign: optical interferometer results. Annales Geophysicae 8, 409–418.

Biondi, M.A., Sazykin, S.Y., Fejer, B.J., Meriwether, J.W., Fesen, C.G., 1999. Equatorial and low-latitude thermospheric winds: measured quiet time variations with season and solar flux from 1980 to 1990. Journal of Geophysical Research 104, 17,091–17,106.

Daniell, R.E, Brown, L., Anderson, D., Fox, M., Doherty, P., Decker, D., Sojka, J., Schunk, R., 1995. PIM: A global ionospheric parameterization based on first principles models. Radio Science 30, 1499–1510.

Fesen, C.G., Crowley, G., Roble, R., Richmond, A., Fejer, B., 2000. Simulation of the pre-reversal enhancement in the low latitude vertical ion drifts. Geophysical Research Letters 27, 1851–1854.

Hedin, A.E. et al., 1991. Revised global model of thermosphere winds using satellite and ground based observations. Journal of Geophysical Research 96, 7657–7688.

Hedin, A.E., Mayr, H.G., 1973. Magnetic control of the near equatorial neutral thermosphere. Geophysical Research Letters 78, 1688–1691.

Martyn, D.F., 1953. Electric currents in the ionosphere: ionization drift due to winds and electric Fields. Philosophical Transactions of the Royal Society, London, Series A 246, 306.

Mendillo, M., Tyler, A., 1983. Geometry of depleted plasma regions in the equatorial ionosphere. Geophysical Research Letters 88, 5778–5782.

Meriwether, J.W., Biondi, M.A., Herrero, F.A., Fesen, C.G., Hallenback, D.C., 1997. Optical interferometric studies of the nighttime equatorial thermosphere: enhanced temperature and zonal wind gradients. Journal of Geophysical Research 102, 20,041–20,058.

Raghavarao, R., Suhasini, R., Hoegy, W.R., Mayr, H.G., Wharton, L., 1998. Local time variation of equatorial temperature and zonal wind anomaly. Journal of Atmospheric and Solar-Terrestrial Physics 60, 631–642.

Raghavarao, R., Wharton, L.E., Spencer, N.W., Mayr, H.G., Brace, L.H., 1991. An equatorial temperature and wind anomaly (ETWA). Geophysical Research Letters 18, 1193–1196.

Richmond, A.D., Ridley, E., Roble, R., 1992. A thermosphere/ionosphere general circulation model with coupled electrodynamics. Geophysical Research Letters 19, 601–604.

Rishbeth, H., 1971. Polarization fields produced by winds in the equatorial F-region. Planetary Space Science 19, 357–369.

Rishbeth, H., 1972. Thermospheric winds and the F-region: a review. Journal of Atmospheric and Terrestrial Physics 34, 1–47.

Schunk, R., Nagy, A., 2000. Ionospheres: Physics, Plasma Physics, and Chemistry. Cambridge Atmospheric and Space Science Series.

Semeter, J., Mendillo, M., Baumgardner, J., Holt, J., Hunton, D., Eccles, V., 1996. A study of oxygen 6300 Å airglow production through chemical modification of the nighttime ionosphere. Journal of Geophysical Research 101, 19,683–19,699.

Wang, W., Killen, T.L., Burns, A.G., Roble, R.G., 1999. A high-resolution, three-dimensional, time dependent, nested grid model of the coupled thermosphere–ionosphere. Journal of Atmospheric and Solar-Terrestrial Physics 61, 385–397.

Wu, Q., Killen, T.L., Spencer, N.W., 1994. Dynamics Explorer 2 observations of equatorial thermospheric winds and temperatures: Local Time and longitudinal dependence. Journal of Geophysical Research 99, 6277–6288.